https://doi.org/10.1016/j.nanoen.2016.08.038 This is the Pre-Published Version.

Ultrathin and Flexible Perovskite Solar Cells with Graphene Transparent Electrodes

Zhike Liu,[a,b] *Peng You,*[a] *Chao Xie,*[a] *Guanqi Tang*[a] *and Feng Yan*[a,*]

[a] Department of Applied Physics, The Hong Kong Polytechnic University, Hung Hom, Kowloon, Hong Kong

[b] Shaanxi Engineering Lab for Advanced Energy Technology, School of Materials Science and Engineering, Shaanxi Normal University, Xi'an, 710119, P. R. China

* Corresponding Authors;

E-mail address: apafyan@polyu.edu.hk;

© 2016. This manuscript version is made available under the CC-BY-NC-ND 4.0 license https://creativecommons.org/licenses/by-nc-nd/4.0/.

Abstract

Flexible and light weight perovskite solar cells have attracted much attention recently for their broad potential applications especially in wearable electronics. However, highly flexible devices cannot be realized with the conventional transparent electrodes based on conductive oxides since they are rigid and brittle. Here, we demonstrate the fabrication of ultrathin and flexible perovskite solar cells with graphene transparent electrodes for the first time. The flexible devices with the structure of polyethylene terephthalate/graphene/poly(3-hexylthiophene)/$CH_3NH_3PbI_3$/$PC_{71}BM$/Ag are prepared on 20 μm-thick polyethylene terephthalate substrates by low-temperature solution process, which show the power conversion efficiency of 11.5% and high bending durability. Moreover, the devices demonstrate the power output per weight (specific weight) of about 5 W/g, which is much higher than those of conventional inorganic solar cells. This work paves a way for preparing flexible perovskite solar cells as well as other optoelectronic devices by using graphene transparent electrodes.

Keywords: Graphene; flexible electronics; perovskite solar cell; transparent electrode

Introduction

Perovskite solar cell (PSC) has been emerged as one of the most promising photovoltaic technologies in recent years. In the past few years, the power conversion efficiencies (PCEs) of PSCs have been rapidly improved from 9% to above 20% [1-4], which are currently comparable to that of commercialized Si-based solar cells while the cost of the PSCs can be much lower due to their convenient fabrication process. To further decrease the cost, PSCs can be prepared by roll-to-roll processes on flexible and light-weight substrates at low temperatures [5-12]. On the other hand, flexible solar cells are expected to have broad potential applications, including wearable or portable electronics, sun-powered vehicles, unmanned airplanes, etc [12,13]. One major challenge in realizing a high-performance flexible PSC is to obtain an ideal flexible transparent electrode, which should be mechanically flexible, bending durable, highly conductive and transparent. Flexible PSCs have been prepared by using various transparent electrodes based on indium tin oxide (ITO) [5], poly(3,4-ethylenedioxythiophene):poly(styrenesulfonate)(PEDOT:PSS) [6,12], aluminum doped zinc oxide (AZO)/silver (Ag)/AZO [7], metal foils [8] and so on. However, conventional ITO transparent electrodes are fragile and thus not suitable for flexible PSCs. The PEDOT:PSS-based transparent electrodes are hydroscopic and can absorb water from the atmosphere to decompose the perovskite layers and consequently degrade the device performance rapidly [14]. Hence, more suitable flexible transparent electrodes for flexible PSCs are urgently needed.

Graphene has been regarded as a promising candidate for flexible transparent electrodes due to its high transparency in broad wavelength region, ultrahigh carrier mobilities and chemical and mechanical robustness [15]. Large-area graphene can be conveniently prepared by chemical vapor deposition (CVD) methods and transferred onto target substrates by roll-to-roll processes [16, 17]. A single-layer graphene film has transmittance of ~97.7% in the visible region, which is much higher than that of a conventional ITO transparent electrode [17]. More importantly, graphene exhibits excellent mechanical flexibility and bending durability, and is thus an ideal candidate for flexible transparent electrodes of flexible PSCs [18, 19]. Although CVD graphene has been used in PSCs on rigid substrates with reasonable efficiencies [20-22], the application of graphene electrodes in flexible PSCs has not yet been reported until now, which requires the devices to be prepared by all-solution processes on flexible plastic substrates at low temperature. Here, we report the fabrication of flexible PSCs with CVD graphene as bottom transparent electrodes on 20-μm-thick polyethylene terephthalate (PET) substrates. To improve the device performance especially the stability of the devices in air, we used hydrophobic poly(3-hexylthiophene) (P3HT) as the hole transport layer (HTL) in the devices [23]. The flexible PSCs show good bending durability and air stability due to the optimal device design and the high flexibility of the graphene electrodes.

Experimental

Materials

$PbCl_2$ was purchased from Alfa Aesar. CH_3NH_3I was synthesized in the lab according to literature procedure. PEDOT:PSS and PCBM were purchased from Clevious and Nano-C, respectively. P3HT was purchased from Rieke Metals Inc.

Preparation of PSCs on ITO electrodes

ITO/glass substrates were coated with PEDOT:PSS aqueous solution (CLEVIOS^{TM} P VP Al 4083) or P3HT (Rieke Metals Inc.) dissolved in chlorobenzene (Anhydrous, Sigma-Aldrich) with different concentrations at 4000 rpm for 40 s, and subsequently annealed at 150 ^{o}C for PEDOT:PSS film and 120 ^{o}C for P3HT film, respectively. After cooling down the substrates, the perovskite precursor solution (CH_3NH_3I: 0.2 g, PbI_2: 0.578 g in 1 ml mixture of anhydrous DMF and DMSO) was spin coated at 4000 rpm for 60 s, during the spin-coating process, 100 μl of chlorobenzene was slowly dripped on the rotating substrate before the surface changes to turbid to obtain a highly uniform and dense perovskite film, Then the substrate was annealed at 50 ^{o}C for 1 min and a higher temperature (80 ^{o}C or 90 ^{o}C or 100 ^{o}C or 110^{o}C) for 2 min. After that, the ETL was prepared by spin-coating a solution of $PC_{71}BM$ (25 mg/ml) at 1500 rpm for 60 s, and annealed at 90 ^{o}C for 20 min to let $PC_{71}BM$ crystallize and diffuse into the perovskite layer. Finally, devices were completed with the evaporation of Ag top electrodes through a shadow mask. The area of the PSC is

designed to be about 4 mm^2.

Preparation of flexible PSCs with graphene electrodes

Single-layer graphene was synthesized on copper foils by CVD method. A layer of polymer, poly(methyl methacrylate) (PMMA) (~300 nm) or P3HT, was spin-coated on graphene and then annealed at 90ºC for 30 min as supporting layer. The polymer coated graphene was obtained after etching of Cu foil in aqueous ammonium persulfate solution, which was washed with DI-water for three times and transferred onto another graphene on the Cu foil. The Cu foil acts as a temporary substrate, and the ammonium persulfate etching was repeated to form a 2-layer-graphene (2L-G)/Polymer film. The 2L-G/polymer film was then transferred onto a PET substrate and the polymer (PMMA or P3HT) film was removed by rinsing it with acetone or chlorobenzene for 3 times. To decrease the surface roughness of the PET substrates, a thin layer of cross-linkable olefin-type polymer (ZEOCOAT™ ES2110) with the thickness of ~2 μm was coated on the surface before the transfer of the graphene layers. Then PEDOT:PSS aqueous solution (added 0.1 wt% Zonyl FSO fluorosurfactant) or P3HT chlorobenzene solution was coated on 2L-G/PET substrates as HTL with the thickness of about 40 nm and 20 nm, respectively. Then other parts of the PSCs with graphene bottom electrodes including perovskite layer, $PC_{71}BM$ film and Ag electrode are prepared at the same conditions for PSCs with ITO electrodes.

Material and device characterization

The contact angles of the PEDOT:PSS and P3HT solutions on graphene surface were measured using a standard goniometer (Rame-Hart Inc.) equipped with a microscope and illumination system. The sheet resistance of graphene films was characterized with a four-probe test system. Scanning electron microscopy (SEM) images of thin films were obtained under a Hitachi S-4300 microscope. The transmittance spectra of graphene films and flexible substrates were measured by using a UV-Vis spectrophotometer (UV-2550, Shimadzu, Japan). The surface of graphene was characterized by atomic force microscopy (AFM, Digital Instruments) and Raman spectroscopy (HORIBA JOBIN YVON, HR800) to check the quality.

The current density versus voltage (*J-V)* characteristics of the PSCs were measured by using a Keithley 2400 source meter under the illumination of a AM 1.5 solar simulator with the light intensity of 100 mW/cm^2 (Newport 91160, 300W) and scan rate was 30 mV/s. The light intensity was calibrated with a standard silicon solar cell. The external quantum efficiencies (EQEs) of the PSCs were measured with a standard test system, including a xenon lamp (Oriel 66902, 300 W), a Si detector (Oriel 76175_71580), a monochrometor (Newport 66902) and a dual channel power meter (Newport 2931_C).

Results and Discussion

Figure 1a shows the schematic diagram of our flexible PSCs with the device

structure of PET/graphene/P3HT/$CH_3NH_3PbI_3$/$PC_{71}BM$/Ag. In our experiments, large-area graphene was prepared by the conventional CVD method and transferred to flexible PET substrates. The bottom graphene electrodes were modified with P3HT films as HTLs. It is notable that P3HT is a p-type semiconductor with suitable energy levels in the PSCs, as shown in **Figure 1b**. P3HT is insoluble to the solvents of perovskite films (dimethylformamide (DMF) and dimethyl sulfoxide (DMSO)), making it possible to prepare the devices with P3HT layers beneath the perovskite layers. In comparison with the typical hole transport polymer PEDOT:PSS, P3HT has the following advantages in the application as HTLs in flexible PSCs. Firstly, P3HT can be uniformly coated on the graphene surface although graphene has low surface energy. As shown in **Figure 1c**, P3HT chlorobenzene solution shows a much lower contact angle (2.6°) than PEDOT:PSS aqueous solution (91.4°) on graphene and thus P3HT can form a much more uniform film on graphene surface than PEDOT:PSS (See Supporting Information, **Figure S1**). Secondly, since the valence band energy level of the perovskite $CH_3NH_3PbI_3$ is -5.4 eV, P3HT has a more suitable highest occupied molecular orbital (HOMO) level (-5.2 eV) than PEDOT:PSS (-5.0 eV) in the application as HTLs in PSCs and can result in higher open circuit voltages of the devices than the latter [24]. Thirdly, P3HT is hydrophobic and will not absorb moisture in air, which is favorable to the stability of PSCs in air [23].

Single-layer CVD graphene was grown on a Cu foil and then transferred onto a flexible PET substrate by a conventional method in the following steps [25]. First, a

thin PMMA layer is spin-coated on the graphene layer followed by etching the Cu foil with the aqueous ammonium persulfate solution. To improve the conductivity of the graphene electrode, a multilayer graphene film can be prepared by stacking the PMMA/graphene film onto another graphene film on Cu foil and then the Cu foil is etched by ammonium persulfate solution. The process is repeated for several times until the required number of layers is obtained. In the end, the graphene film is transferred on a flexible substrate followed by the removal of PMMA with acetone. However, multilayer graphene films show decreased transmittance with the increase of layer number [17], which will affect the light absorption of the active layers in PSCs. According to our previous experience, two-layer graphene electrodes normally show the best performance because of the compromised conductivity and transmittance [26]. Therefore, two-layer graphene electrodes are used in our devices, which can show the transmittance of about 95% in the visible region. One major difficulty in the graphene transfer process is how to completely remove PMMA on graphene surface [27]. We found that P3HT can replace PMMA in the graphene transfer process and better graphene quality can be obtained (see supporting information, **Figure S2**), which has never been reported before. The P3HT-transferred graphene film is much cleaner especially at the edge than the PMMA-transferred ones, which is critical to the quality of the HTL and perovskite layer coated on the graphene surface sequentially. The atomic force microscopy (AFM) image of a transferred graphene also demonstrates that the graphene film is clean, without polymer left on

the surface. The Raman spectrum of the transferred graphene indicates that the graphene film is predominantly single-layer (see supporting information, **Figure S3**) [25].

More importantly, the graphene films show lower sheet resistance when they are transferred by using P3HT, as shown in **Figure 1d**. To understand this effect, we prepared graphene transistors with the two transfer methods and characterized the device performance (see supporting information, **Figure S4**). We can find that the carrier mobilities of the graphene films prepared by the two methods are very similar. However, the Dirac point of the transfer curve (I_{DS} vs. V_G) of the graphene transistor prepared with P3HT method is shifted to a positive gate voltage (~30V), indicating a p-type doping effect in the graphene layer. The conductance of the graphene films can be easily calculated at the gate voltage of V_G = 0V, as indicated by the vertical dash line in **Figure S4**. Hence, the graphene film prepared with the P3HT method can show a higher conductance than that prepared with the PMMA method. This effect can be attributed to the following reason. Since P3HT is a p-type semiconductor, even a ultrathin layer of P3HT remained on the graphene film can induce a p-type doping in graphene and consequently increase the graphene conductance. Therefore, the graphene electrodes are transferred by using P3HT instead of PMMA in our following experiments.

To optimize the fabrication condition, we firstly fabricated PSCs with P3HT HTLs on ITO glass substrates by a solvent-engineering technology [28]. The

schematic diagram and energy structure of planar PSCs are shown in **Figure 2a** and **2b**. The perovskite films were deposited with the precursor of the mixture of PbI_2 and methyl ammonium iodide (MAI) (1:1 mol%) in DMF solution, followed by a chlorobenzene drip during spinning. Chlorobenzene can rapidly reduce the solubility of perovskite materials in DMF for its immiscible property, and all constituents are immediately frozen into a uniform and dense layer at room temperature. Then, the perovskite films are crystallized by thermal annealing at 100 ^oC for 2 min. As shown in **Figure S5** in the Supporting Information, the average grain size of the compact perovskite film is several hundred nanometers, which is a suitable size for flexible PSCs [29]. Next, $PC_{71}BM$ electron transport layer (ETL) is coated on the perovskite layer and annealed at 90^oC for 20 min, which is expected to passivate traps in the device [30, 31]. Finally, Ag top electrodes are evaporated on the devices through a shadow mask with the active area of about 4mm^2.

The thickness of P3HT was optimized by changing the concentration of P3HT solution due to the following reasons. First, the transmittance of the P3HT/ITO layer decreases with the increase of the P3HT thickness due to the light absorption of P3HT in the visible region, as shown in **Figure 2c**, which can influence the light absorption of the active layer. Second, too thin P3HT layer can lead to a low open circuit voltage due to the incomplete coverage on the ITO electrode. The best device performance is thus obtained with the intermediate thickness of P3HT layer (thickness: ~8nm), leading to the maximum PCE of 14.6% (see supporting information, **Figure S6** and

Table S1). Notably, the champion device with P3HT HTL exhibits negligible hysteresis and the similar photovoltaic parameters for the forward and reverse scans, which can be attributed to the high quality perovskite film with few traps prepared on the P3HT film.

To further improve the performance of PSCs, DMSO solvent was added into the perovskite precursor solution (PbI_2:MAI in DMF). It has been reported that DMSO in PbI_2:MAI precursor solution plays an important role in forming high-quality perovskite films [32]. DMSO can combine with PbI_2:MAI to form a MAI-PbI_2-DMSO intermediate phase, which retards the rapid reaction between PbI_2 and MAI during the evaporation of DMF in the spin-coating process [33]. Based on the MAI-PbI_2-DMSO phase, an extremely homogeneous flat film can be obtained. However, excess DMSO will result in thin perovskite layers that cannot absorb sufficient incident light and consequently lead to low photocurrents of the devices. **Figure 2d** shows current density versus voltage (*J*-*V*) curves of the PSCs with different molar ratio of MAI:PbI_2:DMSO. The introduction of DMSO can influence the short circuit current (J_{sc}), fill factor (*FF*) and the open circuit voltage (V_{oc}) of the devices. However, the external quantum efficiency (EQE) of the device decreases with the increase of DMSO ratio due to the decreased film thickness as shown in **Figure 2e**. Therefore, the optimum molar ratio of the PbI_2:MAI:DMSO precursor in the device fabrication is 1:1:2, which leads to a device with J_{sc} of 19.87 mA/cm^2, V_{oc} of 1.04 V, *FF* of 76% and PCE (η) of 15.7%. The device shows good stability, little

hysteresis and a stabilized PCE of 15.4% characterized at the bias voltage (0.86V) for the maximum output power, as shown in **Figure S7**. Ten devices are prepared at the same conditions and the average PCE of 15.68 % is obtained, in which the champion device shows the PCE of 16.24% (See supporting information, **Figure S8** and **Table S2**). In comparison, the PSCs with PEDOT:PSS as HTLs prepared at the same condition show the average PCE of 14.0% mainly due to the relatively low open circuit voltage V_{oc} (~0.94V), which can be attributed to the big difference between the valence band energy level of $CH_3NH_3PbI_3$ (-5.4 eV) and the HOMO level of PEDOT:PSS (-5.0 eV) (see supporting information, **Figure S9**).

The PSCs without encapsulation were stored and tested in ambient air (humidity:70–80%) to check the device stability. The normalized PCEs versus time for PSCs with P3HT or PEDOT:PSS HTLs are summarized in **Figure 2f**. The devices with PEDOT:PSS HTLs show rapid decreases in PCEs in 12 hours while the devices with P3HT HTLs can retain more than 60% of the initial PCEs after 48 hours. The origin of the fast degradation of the PSCs with PEDOT:PSS HTLs is due to water absorption of the PEDOT:PSS layer, which can decompose the perovskite film as reported before [34]. Therefore, P3HT is a more suitable HTL material than the conventional PEDOT:PSS for flexible PSCs.

As shown in **Figure 3a**, PSCs with graphene transparent electrodes were then prepared on flexible PET substrates. To achieve high flexibility, we used PET films with a thickness of only ~20μm as substrates and prepared the devices at the same

condition of the PSCs on glass substrates as described above. To decrease the surface roughness of flexible PET substrates and improve the adhesion of graphene electrodes on top of it, we coated a layer of cross-linkable olefin-type polymer (ZEOCOAT™ ES2110) as the interlayer film (thickness: ~2 μm) on PET surface before transferring graphene layers [35], which can improve the performance of the flexible PSCs. The olefin-type polymer has many advantages, including a low curing temperature, high transparency, high solvent resistance and very low hygroscopicity. It is notable that ZEOCOAT™ has not been successfully used in flexible solar cells until now although it is effective in flexible organic transistors [35]. As shown in **Figure 3b**, double-layer CVD graphene electrodes on PET substrates show the transmittance of ~ 90% in the visible region. After coating a thin layer of P3HT as a HLT, the transmittance of the film is still higher than 80% in the visible region. **Figure 3c and 3d** show the J-V characteristics and EQE curve of flexible PSCs, respectively. The device with the ZEOCOAT™ layer on the PET substrate demonstrates the PCE of 11.5% and V_{OC} of 1.04 V, while the device without ZEOCOAT™ only shows the PCE of 10.4% and a lower V_{OC} (~0.96V) presumably due to the rough surface of the PET substrate. The detailed photovoltaic parameters are shown in the supporting information, **Table S3**. The PCE of the device is stabilized at 11.4% after tens of seconds (see supporting information, **Figure S10**). Since the substrate is only 20μm thick, the power per unit weight of the device is estimated to be 5.07W/g, which is higher than those of the reported ultrathin solar cells based on inorganic materials (e.g. Si, InP and

$CuIn_xGa_{1-x}Se_2$) [36].

As shown in **Figure 3d**, the EQE of the flexible device in the short wavelength region (<450nm) is lower than that of the device prepared on rigid glass substrate shown in **Figure 2e**. This effect is unrelated to the transmittance of the transparent graphene electrodes. Since the light absorption of a perovskite film increases with the decrease of wavelength [20], the generation of carriers by light occurs at positions closer to the surface of the illumination side at a shorter wavelength. So the generated electrons need to diffuse to the Ag cathode for longer distance. If the electron diffusion length is smaller than the thickness of the active layer, the corresponding EQE curve will exhibit a decreased value with the decrease of wavelength, as shown in Figure 3d. Therefore, our results indicate that the flexible PSCs have higher density of traps and shorter electron diffusion lengths in the active layers in comparison with the control devices prepared on rigid substrates.

As shown in **Figure 4a** and **4b**, the flexible device can be attached to curved surfaces with different curvature and show *J-V* curves with little hysteresis under light illumination. **Figure 4c** shows J_{SC} and PCE (η) of the bent PSC, which decrease with the decrease of bending radius. We consider that the change of the performance can be attributed to the variation of the projected area of the curved device. Given the length of the PSC device is L_0, the projected area S of the rectangular device under light illumination is:

$$S = S_0 \frac{\sin(L_0 / 2R)}{L_0 / 2R} \qquad (1)$$

where S_0 is the area of the device when it is flat, R is the bending radius. Assuming J_{SC} and PCE for the curved device are proportional to the projected area, we can obtain:

$$J = J_0 \frac{\sin(L_0 / 2R)}{L_0 / 2R} \quad (2)$$

$$\eta = \eta_0 \frac{\sin(L_0 / 2R)}{L_0 / 2R} \quad (3)$$

where J_0 and η_0 are the short circuit current and PCE of the flat device, respectively. It is notable that the two curves in **Figure 4c** can be fitted very well with equation (2) and (3), indicating that the projected area of the flexible device is the key factor for the change of the device performance. We also can notice that the bending strain has little effect on the fill factor and open circuit voltage of the device.

Figure 4d and **4e** show the performance of a flexible PSC with good bending durability. The PCE is decreased for about 14% after the bending tests (bending radius is 0.175 cm) for 500 times mainly due to the decrease of the short circuit current J_{SC}. We find that the morphology of the perovskite layer, the graphene electrode and the Ag top electrode in control devices show very little change after the bending test, which is the major reason for the good stability of the device performance. It is notable that the degradation of PCE is proportional to the decrease of J_{SC}, as shown in **Figure 4e**, while FF and V_{OC} have little changes in the bending tests, indicating that the resistance of the graphene electrode is unchanged. Since perovskite material is fragile, we consider that the device degradation can be attributed to the cracking of the perovskite layer under mechanical stress. We do can find some flaws (see Supporting Information, **Figure**

S11, dark flaws between grains) in a perovskite film after a bending test under scanning electron microscopy (SEM). The flaws can prohibit carrier transport, induce more traps in the active layer and thus decrease J_{SC} of the device. To better understand the performance degradation, we prepared devices on a thick PET substrate with the same device design. We can find that the device shows relative bigger degradation in its PCE (see Supporting Information, **Figure S12**). Under optical microscopy, some flaws in the Ag top electrode of the thick device can be observed after a bending test although they are not obvious in ultrathin devices (see Supporting Information, **Figure S13**). So the device degradation for a thick device is mainly due to the cracking of the perovskite active layers as well as the metal electrodes due to the higher strain induced by bending. Therefore, one feasible way to improve the bending stability is to use ultrathin substrates that can lead to lower strain in bending tests.

Although attractive, it is rather difficult to realize high-performance flexible solar cells with graphene transparent electrodes mainly due to the difficulties in handling and modifying the one-atom-thick graphene films. Another reason for the low efficiencies of such devices is the higher sheet resistances of graphene electrodes in comparison with conventional transparent electrodes such as ITO, which can be optimized by introducing ideal preparation conditions and suitable doping techniques of graphene in the future [17, 25]. **Figure 4f** shows the PCEs of the representative flexible solar cells with graphene transparent electrodes [19, 37-39], which are normally lower than the PCEs of the counterparts on rigid substrates. It is noteworthy that the flexible PSCs

reported in this paper show the highest efficiency in these devices due to the optimized device fabrication process and the excellent photovoltaic properties of the organic-inorganic hybrid perovskite material.

Conclusions

In summary, we demonstrate ultra-flexible PSCs with graphene transparent electrodes for the first time, and show the device efficiency of 11.5% and the output power per unit weight of 5.07W/g, which is comparable with that of the best flexible PSCs reported before. We find that P3HT is a suitable material for HTLs in the devices since it can be uniformly coated on the graphene electrodes and exhibits matchable band structure in the PSCs. The device performance can be improved by several novel approaches, including the transfer method assisted by P3HT and the introduction of ZEOCOAT™ layer on thin PET substrates, which have never been reported before. Due to the high bending durability of graphene electrodes, the flexible devices can operate at different bending radius and show little degradation in the device performance during the bending tests. This work paves a way of using graphene transparent electrode in high efficiency flexible PSCs and opens up a bright future for a variety of graphene-based flexible optoelectronic devices.

Acknowledgments

This work is financially supported by the Research Grants Council (RGC) of Hong Kong, China (project number: HKU T23-713/11) and the Hong Kong Polytechnic University (project number: G-YM45, A-PL49).

References

[1] H. S. Kim, C. R. Lee, J. H. Im, K. B. Lee, T. Moehl, A. Marchioro, S. J. Moon, R. Humphry-Baker, J. H. Yum, J. E. Moser, M. Gratzel, N.-G. Park, Sci. Rep., 2 (2012) 591.

[2] G. C. Xing, N. Mathews, S. Y. Sun, S. S. Lim, Y. M. Lam, M.Gratzel, S. Mhaisalkar, T. C. Sum, Science, 342 (2013) 344-347.

[3] S. D. Stranks, G. E. Eperon, G. Grancini, C. Menelaou, M. J. P. Alcocer, T. Leijtens, L. M. Herz, A. Petrozza, H. J. Snaith, Science, 342 (2013) 341-344.

[4] W. S. Yang, J. H. Noh, N. J. Jeon, Y. C. Kim, S. Ryu, J. Seo, S. I. Seok, Science, 348 (2015) 1234-1237.

[5] D. Liu, T. L. Kelly, Nat. Photon., 8 (2014) 133-138.

[6] K. Poorkazem, D. Liu, T. L. Kelly, J. Mater. Chem. A, 3 (**2015**) 9241-9248.

[7] C. Roldan-Carmona, O. Malinkiewicz, A. Soriano, G. MinguezEspallargas, A. Garcia, P. Reinecke, T. Kroyer, M. I. Dar, M. K. Nazeeruddin, H. J. Bolink, Energ. Environ. Sci. , 7 (2014) 994-997.

[8] J. Troughton, D. Bryant, K. Wojciechowski, M. J. Carnie, H. Snaith, D. A. Worsley, T. M. Watson, J. Mater. Chem. A, 3(2015), 9141-9145.

[9] F. Di Giacomo, V. Zardetto, A. D'Epifanio, S. Pescetelli, F. Matteocci, S. Razza, A. Di Carlo, S. Licoccia, W. M. M. Kessels, M. Creatore, T. M. Brown, Adv. Energy Mater., 5 (2015) 1401808.

[10] J. You, Z. Hong, Y. Yang, Q. Chen, M. Cai, T.-B. Song, C.-C. Chen, S. Lu, Y. Liu, H. Zhou, ACS Nano, 8 (2014) 1674-1680.

[11] Y.-F. Chiang, J.-Y. Jeng, M.-H. Lee, S.-R. Peng, P. Chen, T.-F. Guo, T.-C. Wen, Y.-J. Hsu, C.-M. Hsu, Phys. Chem. Chem. Phys., 16 (2014) 6033-6040.

[12] M. Kaltenbrunner, G. Adam, E. D. Głowacki, M. Drack, R. Schwödiauer, L. Leonat, D. H. Apaydin, H. Groiss, M. C. Scharber, M. S. White, N. S. Sariciftci, S. Bauer, Nat. Mater., 14 (2015) 1032-1039.

[13] M. B. Schubert, J. Werner, Mater. Today, 9 (2006) 42-50.

[14] J. A. Christians, P. A. Miranda Herrera, P. V. Kamat, J. Am. Chem. Soc., 137 (2015) 1530-1538.

[15] Z. K. Liu, S.-P. Lau, F. Yan, Chem. Soc. Rev., 44 (2015) 5638-5679.

[16] X. Li, W. W. Cai, J. An, S. Kim, J. Nah, D. Yang, R. Piner, A. Velamakanni, I. Jung, E. Tutuc, S. K. Banerjee, L. Colombo, R. S. Ruoff, Science, 324 (2009) 1312-1314.

[17] S. K. Bae, H. K. Kim, Y. B. Lee, X. B. Xu, J. S. Park, Y. Zheng, J. Balakrishnan, T. Lei, H. R. Kim, Y. L. Song, Y. J. Kim, K. S. Kim, B. Ozyilmaz, J. H. Ahn, B. H. Hong, S. Iijima, Nat. Nanotechnol., 5 (2010) 574-578.

[18] J. Liu, Z. Yin, X. Cao, F. Zhao, A. Ling, L. Xie, Q. L. Fan, F. Boey, H. Zhang, W. Huang, ACS Nano, 4 (2010) 3987-3992.

[19] L. G. D. Arco, Y. Zhang, C. W. Schlenker, K. Ryu, M. E. Thompson, C. W. Zhou, ACS Nano , 4 (2010) 2865-2873.

[20] P. You, Z. Liu, Q. Tai, S. Liu, F. Yan, Adv. Mater., 27(2015) 3632-3638.

[21] F. Lang, M. A. Gluba, S. Albrecht, J. Rappich, L. Korte, B. Rech, N. H. Nickel, J. Phys. Chem. Lett., 6 (2015) 2745-2750.

[22] H. Sung, N. Ahn, M. S. Jang, J.-K. Lee, H. Yoon, N.-G. Park, M. Choi, Adv. Energy Mater., 6 (2016) 1501873.

[23] P. Lin, F. Yan, H. L. W. Chan, Langmuir, 25 (2009) 7465-7470.

[24] J. Liu, Y. Wu, C. Qin, X. Yang, T. Yasuda, A. Islam, K. Zhang, W. Peng, W. Chen, L. Han, Energ. Environ. Sci., 7 (2014) 2963-2967.

[25] Z. K. Liu, J. H. Li, Z. H. Sun, G. Tai, S. P. Lau, F. Yan, ACS Nano, 6 (2012) 810-818.

[26] Z. K. Liu, P. You, S. H. Liu, F. Yan, ACS Nano, 9 (2015) 12026-12034.

[27] X. L. Liang, B. A. Sperling, I. Calizo, G. Cheng, C. A. Hacker, Q. Zhang, Y. Obeng, K. Yan, H. Peng, Q. Li, X. Zhu, H. Yuan, A. R. H. Walker, Z. Liu, L. M. Peng, C. A. Richter, ACS Nano, 11 (2011) 9144-9153.

[28] M. Xiao, F. Huang, W. Huang, Y. Dkhissi, Y. Zhu, J. Etheridge, A. Gray-Weale, U. Bach, Y.-B. Cheng, L. Spiccia, Angewandte Chemie, 126 (2014) 10056-10061.

[29] Y. Li, L. Meng, Y. Yang, G. Xu, Z. Hong, Q. Chen, J. You, G. Li, Y. Yang, Y. F. Li, Nat. Commun., 7 (2016) 10214.

[30] Y. Shao, Z. Xiao, C. Bi, Y. Yuan, J. S. Huang, Nat. Commun., 5 (2014) 5784.

[31] J. Xu, A. Buin, A. H. Ip, W. Li, O. Voznyy, R. Comin, M. Yuan, S. Jeon, Z. Ning, J. J. McDowell, P. Kanjanaboos, J.-P. Sun, X. Lan, L. N. Quan, D. H Kim, I. G. Hill, P. Maksymovych, E. H. Sargent, Nat. Commun., 6 (2014) 7081.

[32] N. Ahn, D.-Y. Son, I.-H. Jang, S. M. Kang, M. Choi, N.-G. Park, J. Am. Chem. Soc., 137 (2015) 8696-8699.

[33] N. J. Jeon, J. H. Noh, Y. C. Kim, W. S. Yang, S. Ryu, S. I. Seok, Nat. Mater., 13 (2014) 897-903.

[34] Y. Han, S. Meyer, Y. Dkhissi, K. Weber, J. M. Pringle, U. Bach, L. Spiccia, Y.-B. Cheng, J. Mater. Chem. A, 3 (2015) 8139-8147.

[35] Y. Fujisaki, H. Koga, Y. Nakajima, M. Nakata, H. Tsuji, T. Yamamoto, T. Kurita, M. Nogi, N. Shimidzu, Adv. Funct. Mater., 24 (2014) 1657-1663.

[36] M. Kaltenbrunner, M. S. White, E. D. Głowacki, T. Sekitani, T. Someya, N. S. Sariciftci, S. Bauer, Nat. Commun., 3 (2012) 770.

[37] S. Lee, J. S. Yeo, Y. Ji, C. Cho, D.-Y. Kim1, S.-I. Na, B. H. Lee, T. Lee, Nanotechnology, 23 (2012) 344013.

[38] Z. K. Liu, J. H. Li, F. Yan, Adv. Mater., 25 (2013) 4296-4301.

[39] H. Park, S. Chang, X. Zhou, J. Kong, T. Palacios, S. Gradečak, Nano Lett., 14 (2014) 5148-5154.

Figure Captions

Figure 1. (a) Schematic diagram and (b) energy diagram of a flexible PSC with the structure of PET/graphene/P3HT/perovskite/$PC_{71}BM$/Ag. ZEOCOAT™ thin layer is modified on PET to change the surface property. (c) Contact angles of P3HT chlorobenzene solution (top) and PEDOT:PSS aqueous solution (bottom) on CVD graphene surfaces. (d) The sheet resistance of one or two layers of CVD graphene transferred by using PMMA or P3HT.

Figure 2. (a) Schematic diagram and (b) energy diagram of PSCs on glass substrates with the structure of glass/ITO/P3HT/perovskite/$PC_{71}BM$/Ag. (c) Transmittance of ITO glass substrates coated with P3HT layers with different P3HT concentrations. (d) Current density versus voltage (*J*-*V*) curves and (e) EQE spectra of the PSCs with different molar ratio of MAI:PbI_2:DMSO. (f) Normalized power conversion efficiencies of the PSCs with PEDOT:PSS (red) or P3HT (black) HTLs as a function of storage time in air.

Figure 3. (a) Photograph of flexible PSCs on 20-μm-thick PET substrates; (b) The transmittance of PET substrates (thickness: 20μm or 200μm) coated with 2-layer CVD graphene and P3HT layers. (c) *J*-*V* curves and (d) EQE spectra of a flexible PSC with the PCE of 11.48 % and a control device (without the ZEOCOAT™ layer) with a lower PCE (10.4%). J_{IN} is the integrated photocurrent according to the EQE and solar spectra.

Figure 4. (a) Photograph of a flexible PSC attached to surfaces with different bending radii. (b) *J-V* curves of the PSC with different bending radii characterized under a solar simulator. (c) PCE (η) and short circuit current (J_{SC}) of the PSC as functions of bending radius. The dash lines are fitting curves with equation (2) and (3). (d) *J-V* curves and (e) PCE (black) and J_{SC} (red) of a flexible PSC in bending tests with different number of bending cycles. (f) The record of the PCEs of flexible solar cells with graphene transparent electrodes in recent years.

Figure 1

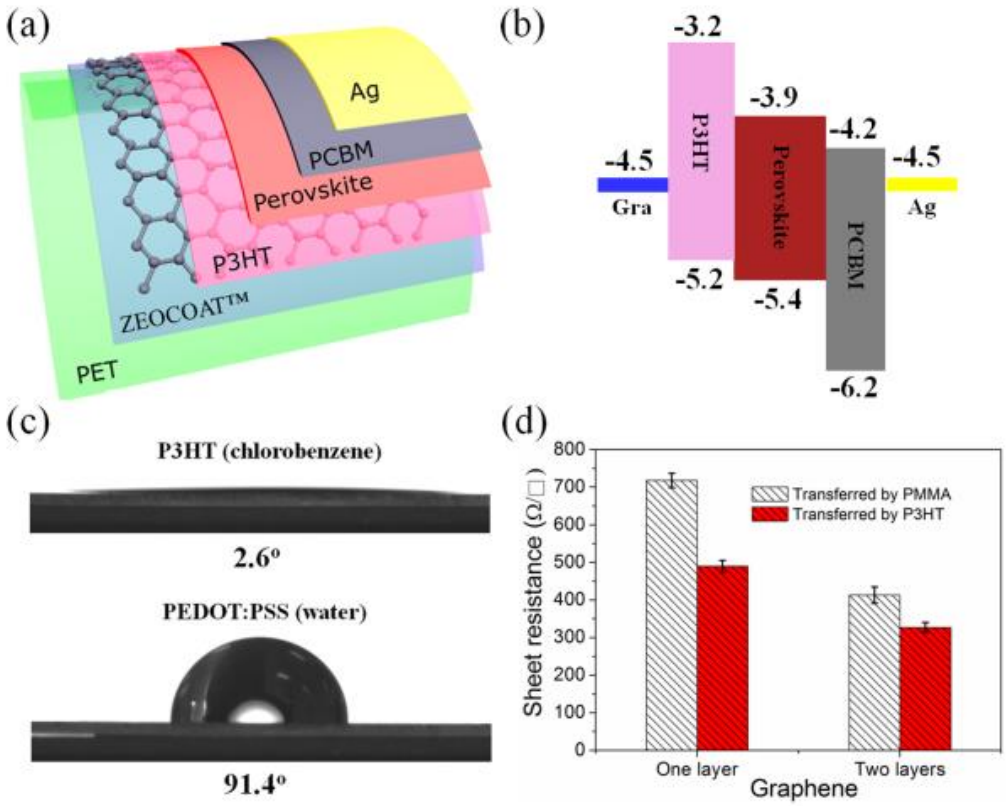

Figure 2

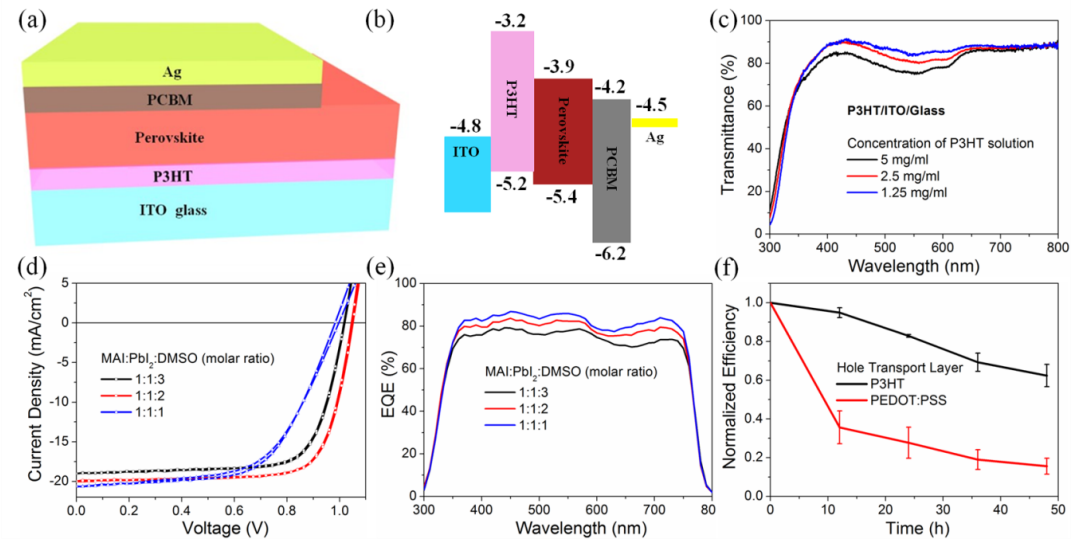
(a)
Ag
PCBM
Perovskite
P3HT
ITO glass
(b)
-3.2
-3.9
-4.2
-4.5
-4.8
-5.2
-5.4
-6.2
ITO
P3HT
Perovskite
PCBM
Ag
(c)
Transmittance (%)
Wavelength (nm)
P3HT/ITO/Glass
Concentration of P3HT solution
5 mg/ml
2.5 mg/ml
1.25 mg/ml
(d)
Current Density (mA/cm²)
Voltage (V)
MAI:PbI2:DMSO (molar ratio)
1:1:3
1:1:2
1:1:1
(e)
EQE (%)
Wavelength (nm)
MAI:PbI2:DMSO (molar ratio)
1:1:3
1:1:2
1:1:1
(f)
Normalized Efficiency
Time (h)
Hole Transport Layer
P3HT
PEDOT:PSS

Figure 3

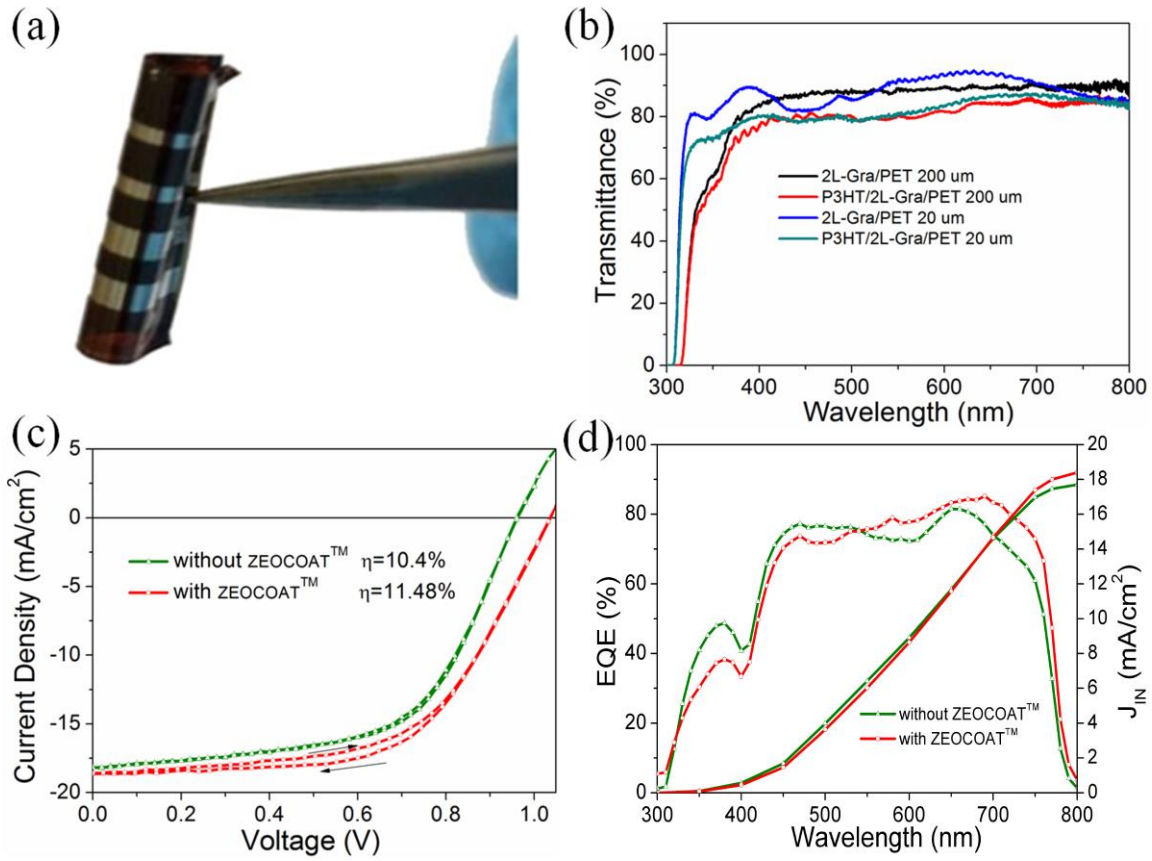
(a)
(b)
Transmittance (%)
Wavelength (nm)
2L-Gra/PET 200 um
P3HT/2L-Gra/PET 200 um
2L-Gra/PET 20 um
P3HT/2L-Gra/PET 20 um
(c)
Current Density (mA/cm2)
Voltage (V)
without ZEOCOAT™ η=10.4%
with ZEOCOAT™ η=11.48%
(d)
EQE (%)
J_IN (mA/cm2)
Wavelength (nm)
without ZEOCOAT™
with ZEOCOAT™

Figure 4

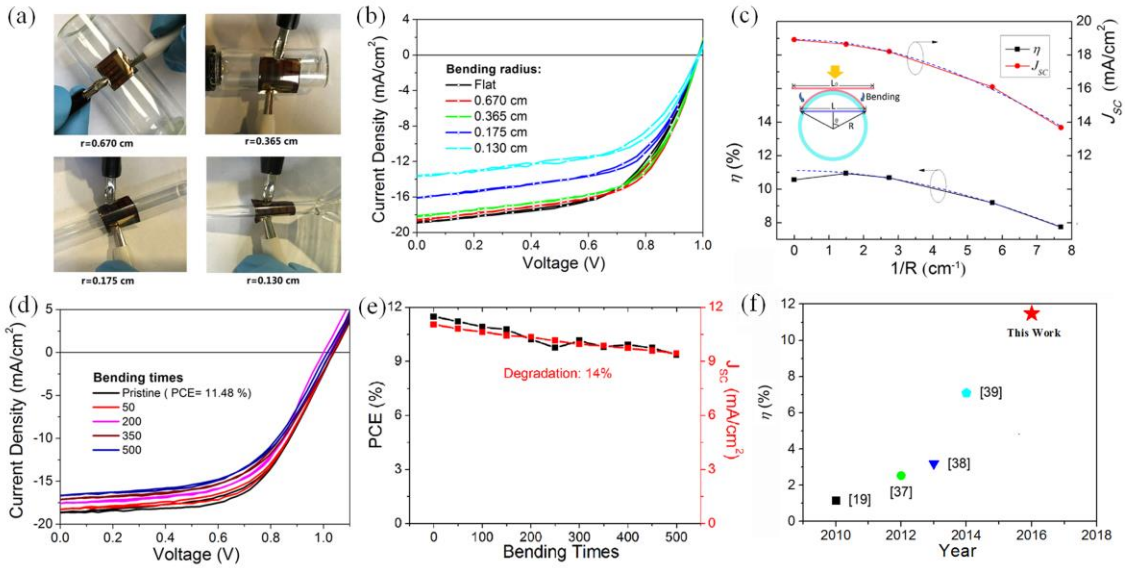
(a)
r=0.670 cm
r=0.365 cm
r=0.175 cm
r=0.130 cm
(b)
Bending radius:
Flat
0.670 cm
0.365 cm
0.175 cm
0.130 cm
Current Density (mA/cm²)
Voltage (V)
(c)
η
J_SC
Bending
η (%)
J_SC (mA/cm²)
1/R (cm⁻¹)
(d)
Bending times
Pristine (PCE= 11.48 %)
50
200
350
500
Current Density (mA/cm²)
Voltage (V)
(e)
Degradation: 14%
PCE (%)
J_SC (mA/cm²)
Bending Times
(f)
This Work
[39]
[38]
[37]
[19]
η (%)
Year

Zhike Liu received his Ph.D. degree from the Department of Applied Physics at Hong Kong Polytechnic University in 2014. He did postdoctoral work at Hong Kong Polytechnic University during 2014–2015. Currently, he is a professor of School of Materials Science and Engineering, Shaanxi Normal University, Xi'an, China. His research is focused on the synthesis, modification and application of graphene for photovoltaic devices.

Peng You received his Master degree in Physics from Qingdao University, China, in 2013. He is a Ph.D candidate in Department of Applied Physics, The Hong Kong Polytechnic University. His research interest is focusing on the fabrication of hybrid perovskite solar cells.

Chao Xie received his B.S. and Ph.D. degrees from Hefei University of Technology in 2009 and 2014, respectively. He is currently a postdoctoral fellow in the Department of

Applied Physics at the Hong Kong Polytechnic University. His research focuses on fabrication of novel electronic/optoelectronic devices based on graphene, perovskite materials and silicon nanostructures.

Tang Guanqi received his M.S. degree in 2015 from Shandong University. Thereafter, he joined Dr. YAN Feng's research group in the Department of Applied Physics at the Hong Kong Polytechnic University as a RA. His current research interests focus on device physics and fabrication of high efficient perovskite solar cell.

Prof. Feng Yan has research interests on organic electronics, 2-D materials, biosensors and energy devices. He received his PhD degree in physics from Nanjing University in China. Then he joined the Engineering Department of Cambridge University in Feb 2001 as a Research Associate and joined National Physical Laboratory in UK in April 2006 as a Higher Research Scientist. He joined the Department of Applied Physics of the Hong Kong Polytechnic University in September 2006.

TOC Graphic:

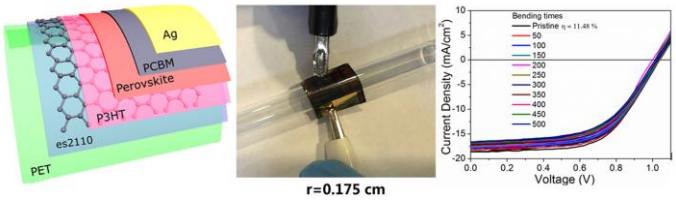
Ag
PCBM
Perovskite
P3HT
es2110
PET
r=0.175 cm
Bending times
Pristine
50
100
150
200
250
300
350
400
450
500
Current Density (mA/cm²)
Voltage (V)